Journal of Materials Chemistry A

PAPER

View Article Online
View Journal | View Issue

Cite this: J. Mater. Chem. A, 2015, 3, 6649

SWCNT-intercalated GO ultrathin films for ultrafast separation of molecules†

Shou Jian Gao,[ab] Haili Qin,[a] Pingping Liu[ab] and Jian Jin*[a]

Laminar separation membranes fabricated with two-dimensional nanomaterials have been extensively explored to achieve the separation of molecules and water purification. Herein, single-walled carbon nanotube (SWCNT)-intercalated graphene oxide (GO) ultrathin laminar films are successfully prepared and used for the separation of molecules with sizes greater than 1.8 nm. Nanochannels created by the intercalation of SWCNT into GO layers greatly improve water permeation compared with pure GO films without sacrificing the rejection of nanometer-scale particles and molecules. A SWCNT-intercalated GO film with a thickness of 40 nm can effectively separate Bovine Serum Albumin, cytochrome c, Coomassie Brilliant Blue and Rhodamine B with fluxes of 660–720 L m^{-2} h^{-1} bar^{-1}, which are about 10-fold higher than the fluxes of traditional nanofiltration membranes with similar rejection properties. The films also exhibit high separation efficiencies of 97.4% to 98.7%. Moreover, the SWCNT-intercalated GO films exhibit excellent pH-stabilities when used in extreme pH conditions, and it is superior to most of the ceramic- and polymer-based membranes. The SWCNT-intercalated GO films have a promising potential to be used as advanced separation membranes for water purification and chemical refinement.

Received 16th January 2015
Accepted 16th February 2015

DOI: 10.1039/c5ta00366k

www.rsc.org/MaterialsA

Introduction

Modern industrialization has brought about severe pollution problems, especially water pollution, which widely and deeply harms the environment and people's health.[1,2] Furthermore, even worse, the crisis of drinkable freshwater is further aggravated because of water pollution.[3,4] Molecules at nanometer scales are one of the most important and intractable pollution sources in waste water and are hard to remove. Filtration membranes, such as nanofiltration membranes and reverse osmosis membranes, could reject nanometer-scale particles and molecules, and they have been extensively studied and used for water purification.[5–10] However, the main shortcoming of polymer- or ceramic-based nanofiltration membranes and reverse osmosis membranes are their low permeation fluxes because of their relatively thick separation layer, which cannot quickly treat waste water and provide fresh water for the growing global population.[11–14] Moreover, the polymer-based membranes are easily corroded by strongly acidic, alkaline, and organic solvents.[15,16] Ceramic-based membranes are also usually expensive and brittle.[17] New advanced separation membranes, which are cost-effective and capable of working in a broad range of operating conditions and most importantly with superior permeation and rejection, are thus highly desired.[14,18]

According to the classical Hagen–Poiseuille equation:

$$J = \varepsilon\pi r_p^2 \Delta p / 8\mu L \quad (1)$$

the permeation flux, J, is directly proportion to the square of the membrane pore radius, r_p, and inversely proportion to the total distance, L, of the liquid running through the membrane.[19] An ideal separation membrane for water purification is expected to have a separation layer as thin as possible to maximize the permeation flux and have appropriate pore sizes to obtain an excellent rejection rate.[20,21] However, this is hard to achieve in a filtration system made from traditional membranes. To achieve the abovementioned goals, new types of membranes with advanced structures need to be designed and developed.

Recently, a series of novel functional separation films with ultrathin film thicknesses and very high permeation fluxes have been constructed by various types of nanomaterials such as diamond-like carbon nanosheets,[22] cross-linked proteins,[19] graphene,[23–28] graphene oxide (GO) nanosheets,[29–35] WS_2 nanosheets,[36] MoS_2 nanosheets,[37] and single-walled carbon nanotubes (SWCNTs),[38–40] to achieve different separation purposes. Among these nanomaterials, a GO nanosheet as a mono-atomic and typical two-dimensional nanomaterial offers an encouraging opportunity to fabricate a brand-new laminar separation

[a]Nano-Bionics Division and i-Lab, Suzhou Institute of Nano-Tech and Nano-Bionics, Chinese Academy of Sciences, Suzhou, 215123, China. E-mail: jjin2009@sinano.ac.cn
[b]Nano Science and Technology Institute, University of Science and Technology of China, Suzhou, 215123, China

† Electronic supplementary information (ESI) available: Thickness and lateral size of the as-prepared GO nanosheet; bundle diameter of the SWCNTs used in this work; flexibility of the film; UV-vis absorption of the molecule solutions before and after separation; rejection rates of BSA, Cyt. c, CBB and RB obtained from the molecule concentrations and the volumes of the retentates and original solutions. See DOI: 10.1039/c5ta00366k

membrane with excellent separation efficiency.[41–44] However, the permeation flux of the pure GO film is not high enough to deliver water due to its narrow interlayer spacing. In this work, we report the fabrication of SWCNT-intercalated GO ultrathin laminar films using single-layered GO nanosheets and SWCNTs *via* a simple and facile approach for ultrafast separation of molecules with sizes greater than 1.8 nm. Nanochannels established by SWCNTs in GO layers greatly improve water permeation compared with pure GO film without the rejection of nanometer-scale particles and molecules. A SWCNT-intercalated GO film with a thickness of 40 nm can effectively separate Bovine Serum Albumin (BSA, 5×5 nm^2), cytochrome c (Cyt. c, 2.5×3.7 nm^2), Coomassie Brilliant Blue (CBB, 2.7×1.8 nm^2) and Rhodamine B (RB, 1.8×1.4 nm^2) in an ultrafast manner with permeation fluxes of 660–720 L m^{-2} h^{-1} bar^{-1}, which are about 10 times higher than the fluxes of traditional nanofiltration membranes with similar rejection properties. Moreover, the SWCNT-intercalated GO films exhibit excellent pH-stability when treating waste water under extreme pH conditions, and they are found to be superior to most of the polymer-based or ceramic-based membranes. The SWCNT-intercalated GO films have a great potential for purifying waste water and drinking water composed of pollutant molecules from industries and daily life.

Experimental section

Materials

GO (thickness: ~1 nm, size: 500–800 nm) used in this work was prepared *via* a modified Hummers method. SWCNT (bundle diameter: 5–20 nm, length: 5–30 μm) were a commercial product supplied by Nanjing XFNANO Materials Tech Co., Ltd, China. All the other chemicals used were of analytical grade, commercially available from Shanghai Chemical Reagent Co., Ltd, and used as received without further purification.

Fabrication of SWCNT-intercalated GO films

First, GO/SWCNT dispersions with different mass ratios of SWCNT to GO (0 : 1, 1 : 10, 1 : 4 and 1 : 2) were prepared by mixing and sonicating a certain amount of a GO dispersion (1.12 mg mL^{-1}) and a SWCNT dispersion (0.071 mg mL^{-1}). Then, the SWCNT-intercalated GO films were fabricated by vacuum-filtering the mixed dispersion onto a porous anodic alumina oxide (AAO) membrane with a pore size of 200 nm or a mixed cellulose ester (MCE) membrane with a pore size of 150 nm. The thickness of the film can be controlled by adjusting the amount of GO/SWCNT dispersion to be filtered. A SWCNT-intercalated GO film with a thickness of 40 nm could be obtained when 90 μL of GO/SWCNT dispersion with a SWCNT/GO mass ratio of 1 : 4 was diluted and filtered on an AAO membrane with a size of 2.54 cm^2. The total mass of the SWCNT and GO was 25.5 μg, including 5.1 μg of SWCNT and 20.4 μg of GO. The total mass stays the same when fabricating SWCNT-intercalated GO films with different SWCNT/GO mass ratios and similar thicknesses.

Molecule separation by the SWCNT-intercalated GO films

The separation process was carried out on a vacuum filter apparatus equipped with a SWCNT-intercalated GO film (support: AAO membrane) and was driven by a pressure difference of 1 bar. In general, 40 mL of feed solution of a certain molecule was poured onto the film and 20 mL of permeate solution was collected through the film. Rejection rates of the molecules were calculated using the concentrations of the molecule in the permeates and original solutions using the following equation:

$$R = (1 - C_P/C_O) \times 100\% \quad (2)$$

(where C_P is the concentration of the molecule in the permeates, C_O is the concentration of the molecule in the original solutions), and it is widely adopted to calculate the rejection rate.[22,36] The concentrations of the molecules in permeates were monitored by UV-vis spectroscopy. Data were obtained by three individual films.

Characterization

SEM images were obtained on a field-emission scanning electron microscope (Hitachi S4800, Japan). TEM images were measured on a Tecnai G2 F20 S-Twin field-emission transmission electron microscope. Water contact angles were measured on an OCA20 machine (Data-physics, Germany). UV-vis spectra were measured on a Lambda-25 spectrometer (Perkin-Elmer Inc, USA).

Results and discussion

As schematically shown in Fig. 1a, to fabricate the SWCNT-intercalated GO ultrathin laminar film, a dispersion containing GO nanosheets and SWCNTs is first prepared by mixing them with a certain mass ratio of SWCNT to GO. Then, the SWCNT-intercalated GO film is assembled by vacuum filtration of a certain amount of the GO/SWCNT dispersion on a porous AAO membrane (with a pore size of 200 nm or a MCE membrane with a pore size of 150 nm). During the film formation process, GO nanosheets are interlocked with each other in a parallel manner forming the lamellar structures, and SWCNTs are intercalated in the stacked GO layers establishing the corrugations and nanochannels for fast water delivery, which will significantly improve the water permeation ability compared with that in pure GO films. Because the lateral size of GO nanosheets (300–800 nm, see Fig. S1†) is larger than the bundle diameter of SWCNTs (5–20 nm, see Fig. S2†), GO nanosheets could totally sandwich the SWCNTs, and there is no rejection defect in the SWCNT-intercalated GO film when it is used for the separation of molecules. Fig. 1b is an optical image of the free-standing and transparent SWCNT-intercalated GO ultrathin film floating on the surface of a mixture of acetone–water. The film exhibits good flexibility (Fig. S3†). When the film was fabricated on a MCE membrane, it could be bent to an angle of 180°. When the SWCNT-intercalated GO film is curled in a water–acetone solution and a droplet of acetone is placed onto

its film surface, it spreads out again (Fig. S3d–3f†). During the entire process, no damage is observed indicating that the SWCNT-intercalated GO ultrathin film is highly flexible and robust. As shown in the SEM image (Fig. 1c) of the SWCNT-intercalated GO film, corrugations and nanochannels constructed by SWCNTs could be clearly observed when the mass ratio of SWCNT to GO is 4 : 1. The thickness of this film is about 40 nm as confirmed by the cross-sectional SEM image (the insert in Fig. 1c). Fig. 1d is a typical TEM image of the SWCNT-intercalated GO film, clearly showing that SWCNTs are uniformly intercalated in the film.

Increasing the nanochannels of the SWCNT-intercalated GO ultrathin film by increasing the mass fraction of SWCNT can further improve water permeation flux of the film, but simultaneously give rise to the sacrifice of the rejection rate if the lamellar structures of the film are destroyed by the SWCNTs. In order to obtain the maximum permeation flux with an acceptable rejection rate, SWCNT-intercalated GO ultrathin films with various mass ratios of SWCNT to GO were fabricated, and permeation fluxes and rejection rates while separating a Coomassie Brilliant Blue (CBB) solution were measured. As shown in Fig. 2a and b, when the mass ratio of SWCNT to GO is 1 : 10, bits of corrugations and nanochannels created by the SWCNTs could be observed compared with the smooth film surface of the pure GO film. However, the permeation flux of a 40 nm-thick SWCNT-intercalated GO film fabricated with SWCNT/GO mass ratio of 1 : 10 barely increases when compared with that of a 40 nm-thick pure GO film (see Fig. 2e). When the mass ratio of SWCNT : GO increases to 1 : 4, a mass of corrugations and nanochannels are obtained in the film (Fig. 2c), and the permeation flux increases to 720 ± 50 L m^{-2} h^{-1} bar^{-1} with a slight decrease in the rejection rate (99.1% ± 0.2% for pure GO film and 98.6% ± 0.3% for SWCNT-intercalated GO film). By further increasing the mass ratio of SWCNT : GO to 1 : 2, the rejection rate of CBB decreases to 77.6% ± 0.6% even though the permeation flux increases to 1190 ± 80 L m^{-2} h^{-1} bar^{-1}. The SWCNT-intercalated GO films fabricated with a SWCNT/GO mass ratio of 1 : 4 are thus chosen for the following separation of molecules.

As shown in Fig. 3a, XRD patterns of the SWCNT-intercalated GO film fabricated with a SWCNT/GO mass ratio of 1 : 4 gives a *d*-spacing of 0.823 nm, which is similar to that of the pure GO film (0.789 nm) and that of the SWCNT-intercalated GO film with the mass ratio of 1 : 10 (0.807 nm). This result indicates that the lamellar structures of GO layers are well-maintained in the SWCNT-intercalated GO films. The films fabricated with a SWCNT/GO mass ratio of 1 : 10 and 1 : 4 are hydrophilic with water contact angles (CAs) of 41° ± 5° and 43° ± 5° (Fig. 3b), which are almost the same as that of the pure GO film. This confirms that nearly all the SWCNTs are intercalated in the stacked GO layers, and no SWCNTs are exposed outside the surface of the film. The small depression of water CA for the film fabricated with SWCNT/GO mass ratio of 1 : 4 is mainly ascribed to the increase in the surface roughness generated by the intercalating SWCNTs. When the SWCNT/GO mass ratio increases to 1 : 2, the water CA of the film increases to 55° ± 5°, indicating that some of SWCNTs are exposed to the outside of the surface of the film.

According to the Hagen–Poiseuille equation, permeation flux of a membrane greatly depends on the thickness of its separation layer. By adjusting the amount of the GO/SWCNT dispersion to be filtered, the thickness of the SWCNT-intercalated GO film could be tuned (see details in Experimental section), which determines the permeation of the SWCNT-intercalated GO film. As shown in Fig. 4a, when the film thickness of the SWCNT-intercalated GO film decreases from 160 nm to 40 nm, the

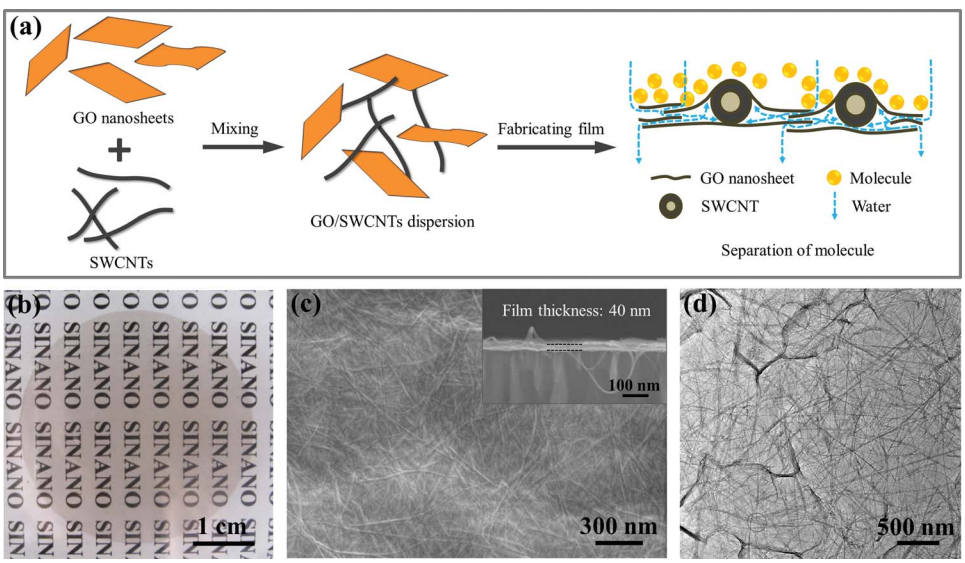

Fig. 1 (a) Schematic showing the fabrication process of the SWCNT-intercalated GO ultrathin film and the process of the separation of molecules. (b) Digital photo of a SWCNT-intercalated GO film floating on the surface of acetone–water solution. (c) SEM image of the SWCNT-intercalated GO film. The inset is a cross-sectional SEM image of the film, showing the film thickness of 40 nm. (d) TEM image of the SWCNT-intercalated GO film.

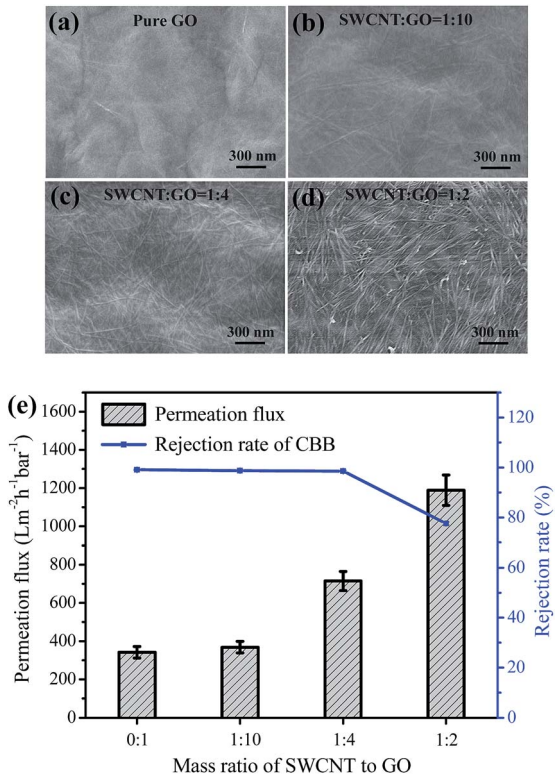

Fig. 2 (a–d) SEM images of the SWCNT-intercalated GO films fabricated with SWCNT/GO mass ratios of 0 : 1, 1 : 10, 1 : 4 and 1 : 2, respectively. (e) Permeation fluxes and rejection rates when separating a CBB solution by the 40 nm-thick SWCNT-intercalated GO films fabricated with different SWCNT/GO mass ratios.

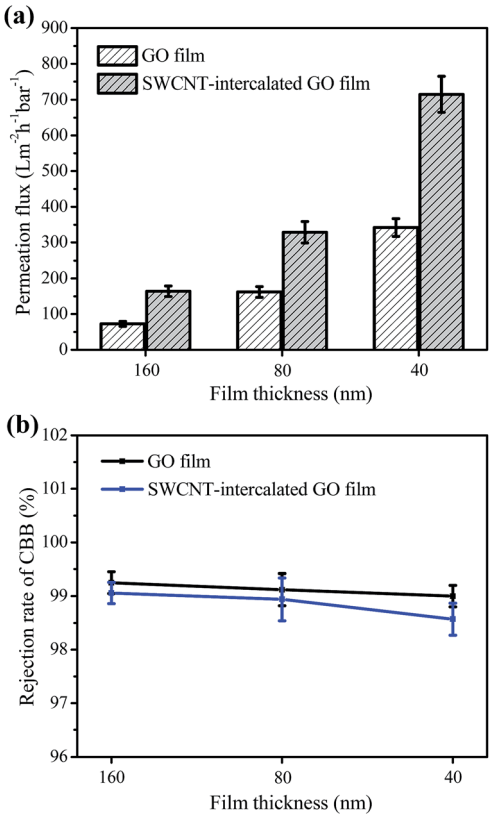

Fig. 4 Variation in permeation flux (a) and rejection rate (b) as a function of film thickness when separating a CBB solution by using the film with a SWCNT/GO mass ratio of 1 : 4.

permeation flux increases from 160 ± 20 L m^{-2} h^{-1} bar^{-1} to 720 ± 50 L m^{-2} h^{-1} bar^{-1} when separating a CBB solution. Moreover, the rejection rate does not decrease significantly (99.0% ± 0.2% for 160 nm-thick film and 98.6% ± 0.3% for 40 nm-thick film) (Fig. 4b).

Table 1 summarizes the separation performance of the 40 nm-thick SWCNT-intercalated GO film. For molecules with sizes greater than 1.8 nm, the film exhibits an excellent rejection rate: 98.7% ± 0.2% for BSA (5 × 5 nm^2), 98.3% ± 0.2% for Cyt. c (2.5 × 3.7 nm^2), 98.6% ± 0.3% for CBB (2.7 × 1.8 nm^2) and 97.4% ± 0.3% for RB (1.8 × 1.4 nm^2). For molecules with sizes less than 1.2 nm, the film cannot effectively separate them from water with the rejection rate of 54.5% ± 0.6% for α-cyclodextrin (α-CD, <1.2 nm) and 30.1% ± 0.5% for $K_3[Fe(CN)_6]$ (0.9 × 0.9 nm^2). To clarify the effect of absorption of molecule on the membrane during filtration, rejection rates using an original feed solution and retentate are also calculated (see ESI, Fig. S4 and Table S1†). Our results show that the rejection rates calculated using either permeate or retentate are close. It indicates that adsorption has little effect on rejection rates, and the rejection in this work is mainly attributed to a molecular-sieving effect.

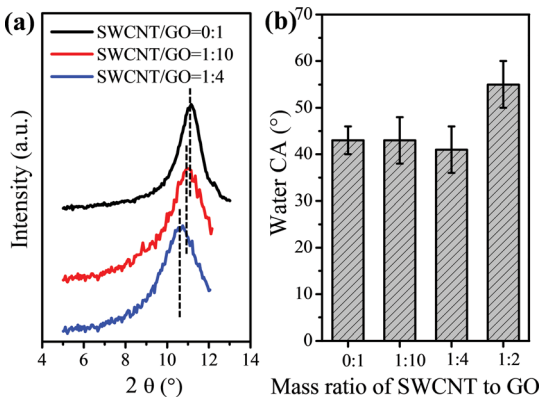

Fig. 3 (a) XRD patterns of SWCNT-intercalated GO films fabricated with a SWCNT/GO mass ratio of 0 : 1, 1 : 10, and 1 : 4. The *d*-spacings are 0.789 nm for the pure GO film, 0.807 nm for a mass ratio of 1 : 10, and 0.823 nm for a mass ratio of 1 : 4. (b) Water CAs of the films with SWCNT/GO mass ratios of 0 : 1, 1 : 10, 1 : 4 and 1 : 2.

Moreover, the film exhibits ultrahigh permeation fluxes for all of the five molecule solutions: 660 ± 30 L m^{-2} h^{-1} bar^{-1} for a BSA solution, 700 ± 50 L m^{-2} h^{-1} bar^{-1} for a Cyt. c solution, 720 ± 50 L m^{-2} h^{-1} bar^{-1} for a CBB solution, 710 ± 50 L m^{-2} h^{-1} bar^{-1} for a RB solution, 640 ± 80 L m^{-2} h^{-1} bar^{-1} for an α-CD solution, and 800 ± 60 L m^{-2} h^{-1} bar^{-1} for a $K_3[Fe(CN)_6]$ solution. These values are about 10-fold higher than the fluxes of traditional nanofiltration membranes with similar rejection properties.[11–14,45–49]

The pH stability of a filtration membrane is very important, especially when treating waste water in acidic or alkaline conditions. The pH stability of our SWCNT-intercalated GO

Table 1 A summary of permeation fluxes and rejection rates for molecules with different diameters by the 40 nm-thick SWCNT-intercalated GO film fabricated with a SWCNT/GO mass ratio of 1 : 4. The rejection rates presented here were obtained from the concentration of molecules in the permeates and original solutions

Molecule	MW (g mol^{-1})	Size (nm)	Concentration	Analyte charge	Permeation (L m^{-2} h^{-1} bar^{-1})	Rejection (%)
BSA	66 430	5 × 5	5 g L^{-1}	−	600 ± 30	98.7 ± 0.2
Cyt. c	12 800	2.5 × 3.7	125 mg L^{-1}	−	700 ± 50	98.3 ± 0.2
CBB	854	2.7 × 1.8	15 mg L^{-1}	−	720 ± 50	98.6 ± 0.3
RB	479	1.8 × 1.4	15 mg L^{-1}	+	710 ± 50	97.4 ± 0.3
α-CD	1127	<1.2	30 mg L^{-1}	N	640 ± 80	54.5 ± 0.6
$[Fe(CN)_6]^{3-}$	212	0.9 × 0.9	15 mg L^{-1}	−	800 ± 60	30.1 ± 0.5

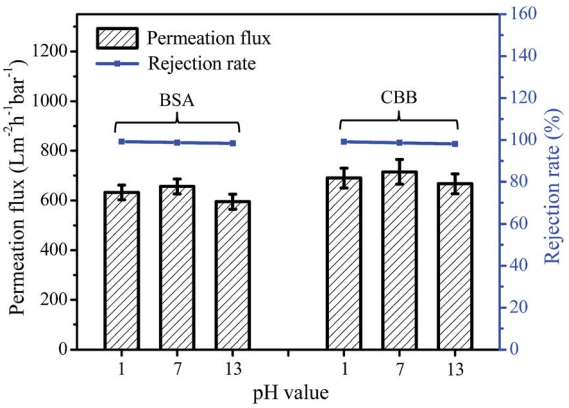

Fig. 5 Permeation fluxes and rejection rates when separating BSA and CBB by a 40 nm-thick SWCNT-intercalated GO film after the film is placed in an acidic solution with pH = 1 or in an alkaline solution with pH = 13 for 7 days.

films is evaluated by monitoring the variation in permeation flux and rejection rate when separating BSA and CBB after the film is maintained in an acidic water solution with pH = 1 or in an alkaline water solution with pH = 13 for 7 days. As shown in Fig. 5, the variations in permeation fluxes and rejection rates with different pH treatments are all very small. These results demonstrate that the SWCNT-intercalated GO film has an excellent pH stability and acid/alkali resistance, which is superior to most of those ceramic-based or polymer-based membranes when treating waste water in acidic or alkaline conditions.

Conclusions

Laminar separation membranes fabricated with two-dimensional nanomaterials have been extensively explored to achieve the separation of molecules. GO nanosheets as a mono-atomic and typical two-dimensional nanomaterial offer an encouraging opportunity to prepare a brand-new laminar separation membrane with excellent efficiency for water purification or gas separation. However, the permeation flux of the pure GO film is still not high enough due to its narrow interlayer spacing for water delivery. Herein, SWCNT-intercalated GO ultrathin laminar films are successfully prepared and used for the ultrafast separation of molecules with sizes greater than 1.8 nm with permeation fluxes of 660–720 L m^{-2} h^{-1} bar^{-1}, which are about 10-fold higher than the fluxes of traditional nanofiltration membranes with similar rejection properties. Nanochannels established by the intercalation of SWCNTs in GO layers greatly improve the water permeation compared with that of pure GO films. Moreover, the lamellar structure of GO layers is well placed to ensure a high rejection rate. This work provides an effective method for designing and fabricating ultrathin GO-based separation films with enhanced performances.

Acknowledgements

This work was supported by the National Natural Science Foundation of China (grant no. 21433012), the National Basic Research Program of China (grant no. 2013CB933000), the Key Development Project of Chinese Academy of Sciences (grant no. KJZD-EW-M01-3), and the Natural Science Foundation of Jiangsu Province (grant no. BK20130007).

Notes and references

1 M. A. Shannon, P. W. Bohn, M. Elimelech, J. G. Georgiadis, B. J. Mariñas and A. M. Mayes, *Nature*, 2008, **452**, 301–310.
2 E. Kintisch, *Science*, 2010, **329**, 735–736.
3 T. Oki and S. Kanae, *Science*, 2006, **313**, 1068–1072.
4 J. Yeston, R. Coontz, J. Smith and C. Ash, *Science*, 2006, **25**, 1067.
5 L. Wang, S. Jin, N. Wang, R. Zhang, G. Zhang and J.-R. Li, *J. Membr. Sci.*, 2014, **452**, 143–151.
6 N. Wang, L. Wang, R. Zhang, J. Li, C. Zhao, T. Wu and S. Ji, *J. Membr. Sci.*, 2015, **474**, 263–272.
7 A. K. Basumatary, R. V. Kumar, A. K. Ghoshal and G. Pugazhenthi, *J. Membr. Sci.*, 2015, **475**, 521–532.
8 Y. Cui, Q. Ge, X.-Y. Liu and T.-S. Chung, *J. Membr. Sci.*, 2014, **467**, 188–194.
9 T. V. Gestel, C. Vandecasteele, A. Buekenhoudt, C. Dotremont, J. Luyten, R. Leysen, B. V. Bruggen and G. Maes, *J. Membr. Sci.*, 2002, **207**, 73–89.
10 L. Yan, Y. S. Li and C. B. Xiang, *Polymer*, 2005, **46**, 7701–7706.
11 A. J. Blok, R. Chhasatia, J. Dilag and A. V. Ellis, *J. Membr. Sci.*, 2014, **468**, 216–223.
12 K. M. Pastagia, S. Chakraborty, S. DasGupta, J. K. Basu and S. De, *J. Membr. Sci.*, 2003, **218**, 195–210.
13 Y. He, G. Li, H. Wang, J. Zhao, H. Su and Q. Huang, *J. Membr. Sci.*, 2008, **321**, 183–189.

14 M. M. Pendergast and E. M. V. Hoek, *Energy Environ. Sci.*, 2011, **4**, 1946–1971.
15 B. V. Bruggen, M. Mänttäri and M. Nyström, *Sep. Purif. Technol.*, 2008, **63**, 251–263.
16 M. Ulbricht, *Polymer*, 2006, **47**, 2217–2262.
17 B. V. Bruggen, C. Vandecasteele, T. V. Gestel, W. Doyen and R. Leysen, *Environ. Prog.*, 2003, **22**, 46–56.
18 D. L. Gin and R. D. Noble, *Science*, 2011, **332**, 674–676.
19 X. S. Peng, J. Jin, Y. Nakamura, T. Ohno and I. Ichinose, *Nat. Nanotechnol.*, 2009, **4**, 353–357.
20 C. C. Striemer, T. R. Gaborski, J. L. McGrath and P. M. Fauchet, *Nature*, 2007, **445**, 749–753.
21 J. K. Holt, A. Noy, T. Huser, D. Eaglesham and O. Bakajin, *Nano Lett.*, 2004, **4**, 2245–2250.
22 S. Karan, S. Samitsu, X. Peng, K. Kurashima and I. Ichinose, *Science*, 2012, **335**, 444–447.
23 L. Qiu, X. H. Zhang, W. R. Yang, Y. F. Wang, G. P. Simon and D. Li, *Chem. Commun.*, 2011, **47**, 5810–5812.
24 D. Cohen-Tanugi and J. Grossman, *Nano Lett.*, 2012, **12**, 3602–3608.
25 K. Sint and N. R. Aluru, *J. Am. Chem. Soc.*, 2008, **130**, 16448–16449.
26 R. R. Nair, H. A. Wu, P. N. Jayaram, I. V. Grigorieva and A. K. Geim, *Science*, 2012, **335**, 442–444.
27 H. Li, Z. Song, X. Zhang, Y. Huang, S. Li, Y. Mao, H. J. Ploehn, Y. Bao and M. Yu, *Science*, 2013, **342**, 95–98.
28 Y. Han, Z. Xu and C. Gao, *Adv. Funct. Mater.*, 2013, **23**, 3693–3700.
29 B. Mi, *Science*, 2014, **343**, 740–774.
30 H. Huang, Z. Song, N. Wei, L. Shi, Y. Mao, Y. Ying, L. Sun, Z. Xu and X. Peng, *Nat. Commun.*, 2013, **4**, 2979.
31 H. Huang, Y. Mao, Y. Ying, Y. Liu, L. Sun and X. Peng, *Chem. Commun.*, 2013, **49**, 5963–5965.
32 P. Sun, M. Zhu, K. Wang, M. Zhong, J. Wei, D. Wu, Z. Xu and H. Zhu, *ACS Nano*, 2013, **7**, 428–437.
33 L. Qiu, X. Zhang, W. Yang, Y. Wang, G. P. Simon and D. Li, *Chem. Commun.*, 2011, **47**, 5810–5812.
34 K. Huang, G. Liu, Y. Lou, Z. Dong, J. Shen and W. Jin, *Angew. Chem., Int. Ed.*, 2014, **53**, 1–5.
35 J. Shen, G. Liu, K. Huang, W. Jin, K.-R. Lee and N. Xu, *Angew. Chem., Int. Ed.*, 2015, **54**, 578–582.
36 L. Sun, Y. Ying, H. Huang, Z. Song, Y. Mao, Z. Xu and X. Peng, *ACS Nano*, 2014, **8**, 6304–6311.
37 L. Sun, H. Huang and X. Peng, *Chem. Commun.*, 2013, **49**, 10718–10720.
38 Z. Shi, W. Zhang, F. Zhang, X. Liu, D. Wang, J. Jin and L. Jiang, *Adv. Mater.*, 2013, **25**, 2422–2427.
39 S. J. Gao, Z. Shi, W. Zhang, F. Zhang and J. Jin, *ACS Nano*, 2014, **8**, 6344–6352.
40 S. J. Gao, Y. Zhu, F. Zhang and J. Jin, *J. Mater. Chem. A*, 2015, **3**, 2895–2902.
41 R. K. Joshi, P. Carbone, F. C. Wang, V. G. Kravets, Y. Su, I. V. Grigorieva, H. A. Wu, A. K. Geim and R. R. Nair, *Science*, 2014, **343**, 752–754.
42 P. Sun, F. Zheng, M. Zhu, Z. Song, K. Wang, M. Zhong, D. Wu, R. B. Little, Z. Xu and H. Zhu, *ACS Nano*, 2014, **8**, 850–859.
43 W. Wang, E. Eftekhari, G. Zhu, X. Zhang, Z. Yan and Q. Li, *Chem. Commun.*, 2014, **50**, 13089–13092.
44 H. Huang, Y. Ying and X. Peng, *J. Mater. Chem. A*, 2014, **2**, 13772–13782.
45 S. Yu, M. Liu, M. Ma, M. Qi, Z. Lü and C. Gao, *J. Membr. Sci.*, 2010, **350**, 83–91.
46 C.-Z. Liang, S.-P. Sun, F.-Y. Li, Y.-K. Ong and T.-S. Chung, *J. Membr. Sci.*, 2014, **469**, 306–315.
47 X. Lia, Y. Chena, X. Hub, Y. Zhanga and L. Hua, *J. Membr. Sci.*, 2014, **471**, 118–129.
48 A. Teella, G. W. Huber and D. M. Ford, *J. Membr. Sci.*, 2011, **378**, 495–502.
49 Y. Liu, S. Zhang, Z. Zhou, J. Ren, Z. Geng, J. Luan and G. Wang, *J. Membr. Sci.*, 2012, **394–395**, 218–229.